A Gray Radiation Aquaplanet Moist GCM. Part II: Energy Transports in Altered Climates

Dargan M. W. Frierson — *UCAR/University of Chicago*

Isaac M. Held — *NOAA/GFDL*

Pablo Zurita-Gotor — *UCAR/GFDL*

Revised Version: August 2006

Abstract

A simplified moist general circulation model is used to study changes in the meridional transport of moist static energy by the atmosphere as the water vapor content is increased. The key assumptions of the model are gray radiation, with water vapor and other constituents having no effect on radiative transfer, and mixed layer aquaplanet boundary conditions, implying that the atmospheric meridional energy transport balances the net radiation at the top of the atmosphere. These simplifications allow us to isolate the effect of moisture on energy transports by baroclinic eddies in a relatively simple setting.

We investigate the partition of moist static energy transport in the model into dry static energy and latent energy transports as water vapor concentrations are increased, by varying a constant in the Clausius-Clapeyron relation. The increase in the poleward moisture flux is rather precisely compensated by a reduction in the dry static energy flux. We interpret these results with diffusive energy balance models. The simplest of these is an analytic model which has the property of exact invariance of total energy flux as the moisture content is changed, but the assumptions underlying this model are not accurately satisfied by the GCM. A more complex EBM that includes expressions for the diffusivity, length scale, velocity scale, and latitude of maximum baroclinic eddy activity provides a better fit to the GCMs behavior.

1. Introduction

In midlatitudes, the poleward transport of heat in the atmosphere dominates over the oceanic contribution (Trenberth and Caron 2001). Dry static energy and moisture fluxes contribute more or less equally to the atmospheric flux (Trenberth and Stepaniak 2003b). Since moisture fluxes play such an important role in the total poleward energy transport, there could potentially be large changes in energy fluxes and hence temperature gradients in climates with increased moisture content. This would include, for example, global warming scenarios or climates such as the Cretaceous. However most of our understanding of the extratropical circulation is based on dry theories. The goal of this study is to improve our understanding of the effect of moisture on energy fluxes and midlatitude eddy dynamics in general.

There are several schools of thinking regarding the effect of moisture on midlatitude atmospheric circulations. On the one hand, moisture serves as an additional source of available potential energy for baroclinic eddies; therefore it is possible that with increased moisture content baroclinic eddies may increase in strength. On the other hand, in terms of the vertically integrated heat budget of the atmosphere, poleward moisture fluxes serve to decrease temperature gradients just as do dry static energy fluxes. If baroclinic eddies are thought of as working off of these temperature gradients, with increased water vapor concentration (and increased meridional fluxes of water vapor) one might expect a decrease in strength of baroclinic eddies.

The theme of ”compensation” between different components of the poleward energy transport, the idea that the total transport is more strongly constrained than individual components, is a recurring one in climate modeling. Manabe and coauthors have studied the changes in energy fluxes under different climate model configurations in several studies. For instance, when the ocean component is removed from a coupled general circulation model (GCM) and replaced by a mixed layer surface, the total (atmosphere plus ocean) energy fluxes are nearly unchanged (Manabe et al. 1975); the atmospheric energy transport increases to compensate the loss of ocean heat flux. When

mountains are removed from a similar atmosphere-only GCM, the total moist static energy fluxes also show little change, even though the partition into stationary eddy and transient eddy fluxes is very different (Manabe and Terpstra 1974). Finally, Manabe et al. (1965) study the removal of moisture from a full GCM, albeit by artificially constraining the static stability in the dry model. Again the moist static energy fluxes are found to be relatively invariant; there is a compensating increase in dry static energy fluxes as the moisture fluxes are removed.

Stone (1978) suggests a very simple framework for understanding the relative invariance of the atmospheric moist static energy fluxes (or total atmosphere plus ocean energy fluxes) in these studies. The claim is that the total poleward energy flux is close to that obtained by assuming that the outgoing long wave radiation (OLR) is independent of latitude, given the observed pattern of absorbed solar radiation. Relatively flat OLR is seen in GCM simulations as well as observations. The claim is that the atmosphere is efficient at flattening the OLR, and it is the proximity to this limit that results in the insensitivity of the total flux.

From another perspective, the determination of poleward energy fluxes is often studied within a diffusive framework. This body of work includes the energy balance model studies of Budyko (1969) and Sellers (1969), and the diffusivity scaling theories of Stone (1972), Green (1970), Held and Larichev (1996), Haine and Marshall (1998), and Barry et al. (2002). The local diffusivity argument is evaluated in a dry quasi-geostrophic model by Pavan and Held (1996). There are alternatives to the diffusive framework. For instance baroclinic adjustment theories predict the temperature structure of the atmosphere (based on neutralizing some measure of baroclinic instability) without references to the fluxes required to give this structure. Diffusive theories in which the diffusivity is a strong function of temperature gradients predict that it is hard to change these gradients, and baroclinic adjustment theories can have the same result. To the extent that the OLR is primarily a function of temperature and the absorbed solar radiation is fixed, the total atmospheric energy transport would be hard to change as well.

Our goal is to evaluate these differing perspectives within an idealized moist GCM by varying

the water vapor content of the atmosphere, and studying the changes in moist static energy fluxes and their partition into dry static energy fluxes and moisture fluxes.

1a. *An Idealized Moist GCM*

Water has a remarkable variety of effects on the climate (Pierrehumbert 2002). We have developed a simplified moist GCM which isolates one of these, the dynamical effect of water vapor through latent heat release, in order to study the interactions of moisture with large-scale dynamics in a framework of relative simplicity.

Complete descriptions of all the physical parameterizations in our model can be found in Frierson et al. (2006), referred to in the following as Part I. We give a brief summary of the parameterizations here. The surface boundary condition is a zonally symmetric aquaplanet with a slab mixed layer ocean of fixed heat capacity, so sea surface temperatures adjust to achieve energy balance in the time mean. There are no ocean heat fluxes in the model, dynamical or prescribed, so the atmosphere performs all the energy transport in the model.

We use a gray radiation scheme in the model, in which the optical depths are fixed and radiative fluxes are a function of temperature alone. There are therefore no cloud- or water vapor-radiative feedbacks. This assumption allows us to study the dynamical impact of increasing or decreasing the water vapor content of the atmosphere in isolation from any radiative effects. We do not claim that the dynamical effects isolated in such a model dominate over radiative effects when, say, the climate is perturbed as in global warming simulations. But we do argue that it is very helpful to isolate the dynamical from the radiative effects in this way in order to build up an understanding of the fully interactive system. The optical depths in the gray scheme are a function of latitude and pressure, which we design to approximate the effect of water vapor in the current climate. The shortwave radiative heating approximates the annual mean net shortwave heating at the top of the atmosphere, and is all absorbed at the surface. There is no annual or diurnal cycle in the model.

Our surface fluxes are calculated from a simplified Monin-Obukhov scheme in which drag coefficients are independent of boundary layer stability provided the surface is unstable, but with reduced drag over stable surfaces. The boundary layer scheme is a standard K-profile scheme with prognostic depth that asymptotes to the diffusivities implied by the Monin-Obukhov scaling near the surface. There is no convection scheme, only large scale condensation when a gridbox becomes saturated. There is additionally reevaporation of any falling precipitation into unsaturated regions below, making the rather extreme assumption that the column must be saturated all the way down for precipitation to reach the ground. There is no condensate in the model. These large scale condensation-only simulations are very similar to simulations we have performed with a moist convective adjustment convection scheme (Manabe et al. 1965). We have additionally developed a simplified Betts-Miller convection scheme for use in this model (Frierson 2006); the results presented here, focused primarily on midlatitude fluxes, are insensitive to the choice of convection scheme unless otherwise stated. We utilize a spectral dynamical core with sigma coordinates, with vertical advection of water vapor by the piecewise parabolic method.

In Section 2, we present results concerning the energy transports as the water vapor content is changed. In Section 3, we interpret the degree of compensation of moisture fluxes by dry static energy fluxes using energy balance models, including a model with the property of exact compensation. We discuss theories for the diffusivity in these energy balance models in Section 4, and conclude in Section 5.

2. Dependence of Energy Transports on Water Vapor Content

We vary the water vapor content of the atmosphere by changing the saturation vapor pressure constant e_0^* which appears in the Clausius-Clapeyron relation

$$e^*(T) = e_0^* e^{-\frac{L_v}{R_v}(1/T - 1/T_0)} \tag{1}$$

The latent heat L_v is independent of temperature and is not varied from experiment to experiment. We find that varying the e_0^* constant is a useful and simple way to vary the moisture content of the atmosphere, with higher e_0^* values used as an analog for warmer climates, and lower e_0^* as an analog for colder climates. In equation 1, we use $T_0 = 273.16\ K$, and the control value of the saturation vapor pressure parameter is $e_0^* = 610.78\ Pa$. We additionally consider cases with $e_0^* = \xi e_0^*(control)$. Experiments with $\xi = 0$ are denoted as the "dry limit", $\xi = 10$ is the 10X case, etc. in the following. The simulations presented here are run for 1080 days, with averages calculated over ever time step of the final 720 days. We have run the following cases at T85 (corresponding to 1.4 degree horizontal resolution) with 25 sigma levels: $\xi = 0, 0.5, 1, 2, 4$ and 10. We have additionally run the cases $\xi = 0, 1$ and 10 at T170 (0.7 degree horizontal resolution) with 25 levels. The climatologies of the T170 cases are presented in detail in Part I. We use extreme values of ξ to better appreciate the effect of water vapor on atmospheric dynamics over a wide parameter range. While the highest and lowest values are extreme, the moisture content in these simulations are perhaps not much more extreme than very cold and very warm climates experienced on Earth, such as the snowball Earth, and the post-snowball hothouse climates, with other paleoclimate regimes and global warming scenarios intermediate.

We next study the poleward fluxes of moist static energy $m = c_pT + gz + L_vq$, dry static energy $s = c_pT + gz$, and latent energy L_vq. The vertically integrated flux of the moist static energy is defined as $2\pi a cos\phi \int_0^{p_s} \overline{vm} dp/g$, where a is the radius of the Earth, ϕ is latitude, and the overbar denotes time and zonal mean. Figure 1 contains the vertically integrated meridional moist static energy (MSE) fluxes, dry static energy (DSE) fluxes, and latent energy fluxes as functions of latitude for $\xi = 0, 1$, and 10 at T170. The intermediate cases $\xi = 0.5, 2$, and 4 are additionally plotted in the DSE and moisture flux plots. As we change moisture content, the moist static energy transport is nearly invariant at every latitude. The moisture transport increases greatly as we increase ξ, but there is a large amount of compensation by the dry static energy fluxes. A useful measure of the degree of this compensation can be obtained from the partition into sensible and latent energy

fluxes at the latitude of maximum total flux. This latitude is approximately the same for all of the simulations; it is always located between 35 and 38 degrees, as is the total (atmosphere plus ocean) poleward heat transport in observations (Trenberth and Caron 2001). The moist static energy flux and dry static energy flux at this latitude are plotted as a function of ξ for all cases in Figure 2. Table 1 lists all the fluxes at the maximum latitude for the T170 cases, and Table 2 contains the T85 cases. At the highest resolution, the amount of compensation (defined by the magnitude of the change in sensible flux divided by the change in latent flux) is almost 99% when going from the dry limit to the control case, and decreases with increasing moisture content (to $\approx 93\%$ when measured from the dry limit to the 10X case). The fluxes are somewhat a function of resolution, especially for the cases with higher moisture content. We note that the compensation increases as resolution is increased. From the top of the atmosphere energy budget, the invariance of the energy fluxes implies that the outgoing longwave radiation is constant as well. We discuss the connection between these quantities, and theories for the compensation in Sections 3 and 4.

The cases with moisture have a well-defined Hadley cell region out to approximately 20 degrees, with strong equatorward transport of moisture, compensated by poleward dry static energy flux. The fluxes within this Hadley cell region only change slightly with moisture content: for instance there is an increase of the maximum equatorward moisture flux of only $\approx 30\%$ from the control case to the 10X case.

Poleward of the Hadley cell, the DSE fluxes decrease and shift poleward as moisture content increases. The 10X DSE fluxes in the extratropics are small (actually becoming slightly equatorward around 30 degrees). The latitude of maximum DSE flux in the extratropics shifts significantly poleward as moisture content is increased, from 36° in the dry limit to 62° in the 10X case (Fig. 1b). The moisture flux maxima all occur at approximately the same latitude as we vary moisture, between 30° and 34° for all cases. The increase in extratropical moisture fluxes is not as rapid as the increase in ξ. Between 20° and 40°, the moisture fluxes are approximately twice as large in the 10X case compared with the control case. This ratio of moisture fluxes between the 10X case and

control case increases to a factor of 7 near the pole.

The actual water vapor concentrations in the model increase more slowly than the increase in ξ, especially in the tropics, for several reasons. One important reason is that lower tropospheric temperatures decrease with increasing moisture. The global mean tropospheric temperatures cannot change much because the insolation is unchanged, the OLR is a function of temperature only, and the average effective level of emission, where OLR = σT^4, is in the midtroposphere. The vertical structure changes are primarily due to changes in the moist adiabat, forcing lower tropospheric temperatures to decrease. Therefore, the column-integrated water only increases by a factor of 5-6 for much of the troposphere from the control case to the 10X case. In addition, the strength of the mean circulation and of the eddies decrease in the high moisture cases. From the control case to the 10X case, the strength of the Hadley cell is reduced by a factor of two, and the maximum eddy kinetic energy in midlatitudes decreases by over a factor of two. These two factors combine to explain the moderate increase in moisture fluxes in midlatitudes. Within the Hadley cell, there is an additional factor which contributes to the very modest increase of the moisture fluxes of only 30% in the 10X case. This additional effect is the moisture content at the outflow level; while negligible for the low moisture cases, the specific humidity outflow for the 10X case is half as much as the lower layer humidities. This results from the strongly decreased lapse rates in the high moisture cases.

Figure 3 gives the decomposition of the total flux into mean and eddy components for the T170 simulations. In observations of the currrent climate, the dry and latent energy fluxes, and the mean and eddy components of these fluxes, combine to create a "seamless" latitudinal profile of the MSE flux (Trenberth and Stepaniak (2003a), Trenberth and Stepaniak (2003b)). As we vary moisture content in these simulations, the partition changes drastically but the sum still creates a seamless profile for the total flux.

While our primary focus here is on midlatitude fluxes, we briefly describe how the Hadley cell fluxes change with ξ. While the total MSE transport varies smoothly in latitude and with ξ, the

component of the MSE transport by the mean Hadley cell varies in subtle ways. The Hadley cell actually transports energy equatorward in parts of the deep tropics in each of these simulations, with equatorward transport over a wider area as moisture concentrations increase. This equatorward flux is balanced by strong eddy moisture fluxes in each of the moist runs, and small eddy fluxes of dry static energy in the dry case, so that the total energy transport is always poleward and smoothly varying with latitude.

A useful diagnostic when studying energy transports by the Hadley cell is the gross moist stability (Neelin and Held 1987), the amount of energy transported per unit mass transport by the circulation, i.e.,

$$\Delta m = \frac{\int_0^{p_s} \bar{v}\bar{m}dp}{\int_{p_m}^{p_s} \bar{v}dp} \tag{2}$$

where Δm is the gross moist stability, m is the moist static energy, p_s is the surface pressure, and p_m is some midtropospheric level (defined so that the equatorward mass flux occurs mostly below, and the poleward mass flux occurs above this level). Since we are considering the zonally and time averaged flow, we can use the meridional velocity as the weights in this calculation, as in Held and Hoskins (1985); using the divergence as a weight, as in Neelin and Held (1987), gives similar results. We plot the gross moist stabilities for the T170 simulations in Figure 4. For the dry limit, the gross moist stability is almost exactly zero at the equator (less than 0.1 K), and increases slowly away from the equator, reaching 5.6 K at 15 degrees. The control case is more strongly negative at the equator (-2.2 K), and becomes positive more quickly away from the equator. The 10X case begins slightly stable at the equator, then becomes negative out to 9 degrees (the asymmetry between hemispheres in these two cases is due to sampling error and the fact that the mass transport in the denominator of this expression approaches zero at the equator). A consistent picture of this behavior and the area of equatorward transport is that a large scale condensation-only model of this resolution creates a highly unstable tropics which transports energy towards the source of the convection, as in CISK theories (Charney and Eliassen 1964), with eddies carrying significant amounts of latent heat poleward. In the dry limit, in contrast, the temperatures are essentially on the

same dry adiabat throughout the tropics, implying zero static stability at the equator, and small eddy fluxes. Not surprisingly, the tropical circulation within this model, with no convection scheme, is sensitive to resolution. This dependence on resolution, and the effect of an idealized convection scheme on the Hadley circulation, gross moist stability, and tropical precipitation distribution are studied in Frierson (2006).

3. Energy Balance Models

We have demonstrated in Section 2 that there is a rather precise compensation between changes in latent energy fluxes and dry static energy fluxes as we vary ξ. We can put into context how precise this compensation is by addressing the argument of Stone (1978) that explains compensation from the flatness of the OLR. Given the net shortwave radiation at the top of the atmosphere, S, and the OLR, I, the moist static energy flux F is

$$F(\phi) = 2\pi a^2 \int_0^{\phi} (S - I) cos\phi^* d\phi^* \tag{3}$$

where ϕ is latitude and a is the radius of the Earth. One might consider the limit in which OLR is flat, in which the atmosphere has managed to remove the temperature gradient at the effective emission level for the OLR, as the maximum sustainable atmospheric flux. This is actually not a strict upper limit in our model; we have generated solutions, with optical depths strongly decreasing polewards, with reversed temperature gradients at the emission level (but not at the surface). However this limit is still interesting to consider. Substituting in the shortwave radiation profile used in our model, and the proper uniform OLR to ensure global energy balance (234.6 $W\ m^{-2}$), one obtains 7.82 PW for the maximum flux. For our idealized GCM, the fluxes are sufficiently far from this limit ($\approx 5.6\ PW$ for $\xi = 0$ and $\xi = 1$) that this cannot be the full explanation for the insensitivity of the total flux to water vapor content.

To help interpret the compensation of energy fluxes, we introduce a one-dimensional energy balance model (EBM) in which all of the energy transport is diffusive (Sellers (1969)). The form

of the energy balance model is

$$\begin{aligned} 0 &= S - I + \tilde{D}\nabla^2 m \\ &= S - I + \frac{\tilde{D}}{a^2 cos(\phi)} \frac{d}{d\phi}\left(cos(\phi)\frac{dm}{d\phi}\right) \end{aligned} \tag{4}$$

where $\tilde{D}$ is the diffusion coefficient. It is related to the kinematic diffusivity D, by $\tilde{D} = p_s D/g$, where p_s/g is the mean mass of an atmospheric column per unit area, which we set equal to $10^4\ kg\ m^{-2}$ when needed. Lapeyre and Held (2003) have obtained results that suggest lower layer values of moist static energy are most appropriate for diffusive models of energy fluxes; therefore we take m to be the moist static energy just above the surface which can be written as

$$m = c_p T_s + L_v q_s = c_p T_s + h_s L_v q_s^* = c_p T_s + h_s L_v \frac{R_d e_s^*}{R_v p_s} \tag{5}$$

where the subscripts s represent surface values, q_s^* is the saturation specific humidity at the surface, h_s is the surface relative humidity, and e_s^* is the saturation vapor pressure calculated using the surface temperature in equation 1. The dependence on ξ comes from the e_s^* expression.

3a. *EBM with Exact Compensation*

The simplest energy balance model we present has the property of exact compensation: energy fluxes do not change as we vary moisture content through the parameter ξ. This model uses the following assumptions in the diffusive energy balance model. First, the diffusivity D does not change as we vary moisture content. Second, the effective level of emission (the level where the temperature equals $(I/\sigma)^{1/4}$, where σ is the Stefan-Boltzmann constant) does not change as we vary ξ. This is an excellent approximation for this GCM since the optical depths in our gray radiation scheme are the same for all of our simulations. Third, we assume that all water vapor has condensed out at the emission level. This assumption seems reasonable since the emission level in our GCM is well above the e-folding depth for water vapor. Finally, we assume that the atmosphere has the same moist static energy at the emission level as it does at the surface. This is

a reasonable starting point, since the moist isentropes in our model are close to vertical from the midlatitudes equatorwards, a key result in Part I.

To prove that the solution of this EBM is independent of ξ, rewrite the EBM as

$$0 = S - \sigma T_E^4 + \tilde{D}\nabla^2 m \tag{6}$$

where T_E is the emission temperature. Using the assumptions that the atmosphere is on a moist adiabat between the surface and the emission level, and that the water vapor is negligible at the emission level, we can relate the surface moist static energy to the temperature at the emission level:

$$c_p T_E = m - g z_E \tag{7}$$

Substituting into the EBM, we have

$$0 = S - \sigma (m - g z_E)^4 / c_p^4 + \tilde{D}\nabla^2 m \tag{8}$$

Nothing in this equation is a function of ξ; therefore there is a unique steady solution for m, the flux of m, and the OLR. Changing ξ only changes the partition of the fluxes into latent and sensible components. We refer to this model as EBM1.

3b. *Refinements to the EBM*

None of the assumptions in EBM1 are exactly true in the GCM. We therefore modify the EBM to understand the GCM further. We first relax the assumption that all moisture has condensed out by the emission level, and calculate actual moist adiabats to get the emission temperature, assuming a surface relative humidity of 80% (an assumption for surface relative humidity is required, and we choose 80% as an approximation to the model simulations and observed surface humidities). We additionally assume that the diffusion coefficient is independent of latitude, and tune its value to match the maximum flux in the control case to that of the GCM. We run the EBM with the emission heights from the control run of the model as input. The emission levels in our model

change little from simulation to simulation since the optical depths for radiation do not change. The emission level peaks at the equator with a value of approximately 6 km, and has a minimum at the poles of 1.5 km. We note that the approximation

$$z_E = 1590 - 700\ cos(\phi) + 5370\ cos^2(\phi) \tag{9}$$

gives an excellent approximation to the control simulation emission level, and can be used to reproduce the results below.

The result of tuning the diffusivity to match the maximum flux in the control case to that of the GCM is $D = 1.84 \times 10^6\ m^2\ s^{-1}$, which produces a good fit to the flux of MSE at all latitudes. We refer to the resulting model as EBM2. The surface moist static energy gradient is close to the GCM value in the control experiment as well. One can compute the partition of the flux into moist and dry parts if one assumes that the fluxes of temperature and water vapor are individually diffusive with the same diffusion coefficient. Making this additional assumption, one finds that the ratio of moisture flux to dry static energy flux is larger than the GCM value. This can be attributed to the neglect of the moist stability, which causes the EBM surface temperatures (and hence the moisture content and moisture gradients) to be slightly too large. However, due to the large increase in complexity that would be needed to model the static stability and its spatial structure, we find this model of the control case adequate. We emphasize that adding a latitudinally constant moist stability to this model keeps the moist static energy flux the same, but does affect the partition into dry and moist components. Therefore we primarily focus on the moist static energy fluxes in the following.

We proceed by using the same diffusion coefficient and emission level profile within the EBM while varying moisture. The maximum fluxes for these cases can be seen along with the GCM values in Figure 5. Clearly we have lost the precise cancellation captured by EBM1. The maximum fluxes now range from 5.26 PW for the dry limit to 7.22 PW for the 10X case. Despite its elegance, we do not believe that EBM1 captures the essense of this precise cancellation, since

the assumptions made in EBM2 with regard to the difference in moist static energy between the surface and the level of emission mimic the GCM more closely.

We now examine the effective diffusivities found in the GCM, both to refine the energy balance model further and to test these values with theories for the diffusivity such as Held and Larichev (1996) and Barry et al. (2002). We define the diffusivity as the vertically averaged flux of moist static energy divided by the gradient of moist static energy at the surface. These effective diffusivities for the T170 cases are plotted in Figure 6 for the extratropics. We have removed the deep tropics from this plot, where the diffusive approximation is not expected to be valid. The values in the tropics are poorly defined, but do not have a large effect on the solution in any case because the MSE flux is small there. When area-averaged over the extratropics (poleward of 25 degrees) the mean diffusivity decreases with moisture content. These mean values of the diffusivity for all cases are plotted in Figure 7. They are somewhat sensitive to the latitudinal domain used for averaging, due to the complex spatial structures. We note however that the value for the control case ($1.87 \times 10^6\ m^2\ s^{-1}$) is very similar to the value which works best in EBM2. The comparison with the T85 cases in Figure 7 demonstrates the relative insensitivity to resolution of the inferred diffusivity, and confirms the gradual decrease of diffusivity as moisture is increased.

We next investigate the sensitivity of EBM2 to the diffusivity, first by calculating the diffusivities required to reproduce the maximum flux in the GCM simulations. Using the T170 simulations only, we find that the values required by the EBM in the 10X case and the dry limit are very close to the actual GCM values. When the control emission height is used for all cases, the required diffusivities are $2.05 \times 10^6\ m^2\ s^{-1}$ for the dry limit, and $1.10 \times 10^6\ m^2\ s^{-1}$ for the 10X case. These required diffusivities for the EBM as a function of ξ are also plotted in Figure 7. The agreement between required EBM diffusivity and the GCM values suggests that a theory for the change in diffusivity is the only remaining component needed to explain the compensation seen in our GCM. Changes in static stability, emission level, and the structure of the diffusivity are secondary to changes in the mean diffusivity in explaining the behavior of the GCM.

To get an idea of the sensitivity of the fluxes to the diffusivity within EBM2, we run this model over a wide range of diffusivities for the dry limit, control case, and 10X case. The maximum moist static energy flux as a function of diffusivity is plotted in Figure 8. Each point on this plot represents one steady state of the EBM. When the diffusivity is small, the fluxes go to zero and the model is in radiative equilibrium. In the other extreme limit, the surface temperature and moist static energy have become homogenized. This corresponds to a reversed OLR gradient due to the emission height structure with latitude. The flux asymptotes to a smaller value for the 10X case due to the reduced temperature lapse rate up to the emission level, creating a smaller OLR reversal, and smaller fluxes. Provided the diffusivity is not very small, the latitudinal structure of the fluxes is very similar over this wide range of diffusivities. The maximum flux always occurs within 2 degrees of 36 degrees provided the diffusivities are greater than $9 \times 10^5\ m^2 s^{-1}$.

It is clear from Figure 8 that the maximum fluxes are quite sensitive to changes in diffusivity at their current state. In fact, each are at approximately their most sensitive point in the domain of diffusivities. The 10X case is most sensitive to diffusivity for small values of diffusivity, due to the strong positive feedback of moisture on surface moist static energy gradients as surface temperature gradients increase. Our conclusion from this plot is that the change in diffusivity from case to case is important for the observed invariance of fluxes. While it is certainly possible that the total flux in this system is somehow constrained to remain nearly unchanged for some other reason, and that the effective eddy diffusivity then adjusts to satisfy this constraint, we do not have a candidate for this constraint and, therefore, continue by examining possible theories for the diffusivity.

4. Theory for Diffusivity

Eddy diffusivity theories are based on the principle that perturbations in the quantity being mixed can be written as a mixing length times the mean gradient of the quantity, in this case, that

$$|m'| = -L_{mix} \frac{1}{a} \frac{\partial \bar{m}}{\partial \phi} \tag{10}$$

Then the eddy diffusivity is calculated as the following:

$$D = kL_{mix}|v'| \tag{11}$$

where k is a correlation coefficient between v' and m, and $|v'|$ is the rms eddy velocity. In the past, theories have been developed using length scales including the Rhines scale (Held and Larichev (1996), Barry et al. (2002)), the Rossby radius (Stone (1972)), the scale with maximum growth in the Charney problem (Branscome (1983), Stone and Yao (1990)), and the width of the baroclinic zone (Green (1970), Haine and Marshall (1998)). These theories have used scales for the velocity fluctuation including the mean zonal wind (Stone (1972), Haine and Marshall (1998)), scales based on equipartition of kinetic and available potential energy (Green (1970)), or scales based on entropy production and the kinetic energy cycle (Barry et al. (2002)).

In Part I, we found that the length scales of eddies in the GCM, measured by the spectrum of the vertically averaged variance of the meridional velocity, are remarkably constant, both with latitude (outside of the tropics), and with changes in moisture, despite the large changes in dry stability and the radius of deformation. One is tempted to view this fixed eddy scale as determined by the fixed geometry, but one can change this length scale, for example, by changing the rotation rate or by changing the baroclinicity, holding ξ fixed. The dynamical interpretation offered in Part I is that the length scale is the Rhines scale at the latitude of maximum eddy kinetic energy. We define this scale to be L_R, with $L_R^2 \equiv |v'|/\beta$. The latitude of maximum eddy energy moves poleward as ξ increases, and the resulting decrease in β at this latitude is essential in order for this theory to fit the GCM data, with a length scale that changes very little as ξ increases. From this perspective, there is nothing fundamental about the insensitivity of the eddy length scale to ξ.

We first investigate whether this length scale times $|v'|$ at the latitude of maximum eddy kinetic energy (EKE) gives an adequate description of the changes in diffusivity. We plot these predicted diffusivities ($kL_R|v'| = k|v'|^{3/2}\beta^{-1/2}$) along with the average GCM diffusivities in Figure 9. A correlation coefficient $k = 0.32$ is chosen to match the T170 control case diffusivity, and this then

is used for all cases. The diffusivities agree well with the GCM for high moisture cases, but diverge slightly at low moisture content.

To complete this expression for the diffusivity (and hence the temperature profile and fluxes from the EBM) one needs a theory for the latitude of maximum EKE, and the RMS velocity at that latitude. In Part I, we show that the static stability can for some purposes be thought of as near neutral in terms of moist stability from the midlatitudes equatorward. However, there is some moist stability in the midlatitudes that increases as moisture is added. Further, the atmosphere is very stable in the polar regions. Lacking a simple unified theory for this behavior, and consistent with the level of complexity of the EBM as presented so far, we investigate whether a useful expression for the diffusivity can be obtained without considering how to determine the moist stability and how this moist stability affects the diffusivity.

The latitude of maximum eddy kinetic energy shifts significantly poleward as the moisture content is increased. The Eady growth rate, $f\partial U/\partial z/N$ has been successfully employed to locate the latitude of midlatitude storm tracks (Hoskins and Valdes 1990). This depends on the stability, but we simply ignore this dependence here and assume that the structure in the meridional temperature gradient is dominant, estimating the position of maximum kinetic energy by locating the maximum in the temperature gradient at 630 hPa. These quantities are plotted in Figure 10. This simple method captures the latitude of maximum EKE quite well. The predicted latitudes are plotted in Figure 11.

Finally, we need an expression for $|v'|$. Stone (1972) assumes

$$|v'| \sim \frac{1}{f}\frac{\partial T}{\partial y} \tag{12}$$

which is equivalent to assuming equipartition between eddy kinetic energy and the mean available potential energy within one radius of deformation, but the end result (Eqn 12) has no explicit dependence on static stability. Since our results are fit far better by assuming that the eddy scale is the Rhines scale (at the latitude of maximum EKE) than with a dry or moist Rossby radius, use of this expression would appear to be inconsistent. However, Schneider (2004) shows in an idealized

dry model that the static stability adjusts to keep the Rossby radius proportional to the Rhines scale, preventing a significant inverse cascade. In our moist model, in which we also do not see a significant inverse cascade, we speculate that there may be an effective moist stability that allows use of this same equipartition argument, although we do not know how to estimate this effective stability independently. If this were true in our model, it suggests that a Rossby radius could be used as a measure of eddy length scales, if we knew the proper static stability to choose.

While our justification is not very solid, we have found no other simple scaling argument that works as well. The expression Eqn 12, using the temperature gradient at 630 hPa at the latitudes of maximum EKE in the GCM (and f at the latitude of maximum EKE in the GCM as well), is compared to the vertical mean GCM $|v'|$ in Figure 12.

We next run the EBM predicting the latitude of maximum EKE, the RMS meridional velocity, the length scale, and the diffusivity. These are predicted at each time step, and the model is run until converged. The equations for this model (EBM3) are made fully explicit in the appendix, where we also describe the tuning process. The results for the fluxes in EBM3 are plotted in Figure 13. Given our level of understanding of closures for moist eddies, this level of agreement is encouraging. Further, the movement of the latitude of maximum EKE is well-predicted by this model, although somewhat exagerated: these are plotted in Figure 11. The predicted RMS velocities can be found in Figure 12, and the diffusivities in Figure 9.

5. Conclusions

We have studied the meridional fluxes of moist static energy as moisture content is increased within an idealized GCM. The moisture fluxes increase with moisture as expected; however there is an accompanying decrease in the dry static energy flux, leaving the total moist static energy flux nearly unchanged, both in terms of structure and magnitude of fluxes. The compensation (change in dry static energy flux divided by change in moisture flux) at latitude of maximum flux is approximately

99% from the dry limit to the control case at T170 resolution. As moisture content increases, the total flux increases slightly, but there is still 93% compensation from the dry limit to the 10X case at T170 resolution. The compensation is remarkable given the large changes in many aspects of the climate among these simulations: as moisture content is increased, the dry stability increases, the jet shifts poleward, the eddy kinetic energy is reduced, and the Hadley circulation weakens.

We investigate the reasons for this compensation within diffusive energy balance models. Energy balance models with diffusivity that is uniform with latitude are able to capture the latitudinal structure of the moist static energy fluxes from the simulations with considerable precision; this is in accordance with the result of Stone (1978) that the structure of the fluxes cannot deviate much from the shape of the fluxes obtained from assuming constant OLR with latitude.

An energy balance model with four assumptions, all of which are approximately satisfied within the full model, has the property of exact compensation as moisture content is changed. This model consists of fixed diffusivity of surface moist static energy, fixed emission level, neutral moist stability between the surface and the emission level, and all moisture condensed out by the emission level. We provide a simple proof for the invariance of fluxes in this case.

The upshot of the latter three of the these assumptions, that the outgoing long wave radiation can be thought of as a function of the surface moist static energy, is not accurately observed by the GCM and, as a result, in order to explain the near-equality of fluxes especially in the higher moisture content cases, one must additionally consider the change in diffusivity with moisture content. The diffusivity is found to decrease by approximately one-third as moisture increases from the control case to the 10X case, and using the GCM values of diffusivity within the EBM gives the proper degree of compensation. As in standard mixing length theories, we write our theory for the diffusivity as the product of a length scale times a velocity scale. The length scale is taken to be the Rhines scale at latitude of maximum EKE, as in Part I. The latitude of maximum EKE is chosen to be the latitude with maximum temperature gradient at 630 hPa. The theory for the velocity scale is based on equipartition of dry mean available potential energy within a

radius of deformation, and eddy kinetic energy. An EBM that includes all of these effects is able to qualitatively reproduce the poleward shift of the jet, the reduction in EKE, the reduction in diffusivity, and near-equality of fluxes with moisture content.

Moisture affects atmospheric static stability, temperature gradients, eddy energies, the latitude of maximum eddy activity, and the relative magnitude of the dry static and moist poleward energy transports. The three energy balance models we have proposed in this work each provide a framework for interpreting changes in these quantities in altered climates, and can be used as a baseline for comparison with full GCM simulations.

A robust poleward shift of the midlatitude storm track with increased temperature/moisture content has been seen in global warming simulations (Yin 2005), and with a full GCM over idealized boundary conditions (Cabellero and Langen 2005). Our results suggest that moisture may be fundamental in determining this shift, but further work is needed to quantify this effect as compared to other mechanisms that can shift the midlatitude circulation polewards.

The energy balance models suggest that the key to the poleward shift in this idealized GCM with increasing moisture is the increase in latent heating in midlatitude storms, this heating being centered equatorward of the storm track, thus shifting the temperature gradient giving rise to the storms further polewards. Alternatively, if one allows oneself to start from the result that the total poleward energy flux changes much less than the latent heat flux, one can argue that the maximum in the dry static energy flux must move polewards in response to the preferential increase in the latent heat flux on the warmer, equatorward side of the storm track. The poleward movement of the storm track then follows if one ties it to the location of the maximum in the dry static energy flux. Effectively, the increase in moisture makes it easier for eddies of the same size to transport energy, but this easing is felt more strongly on the equatorward side, so the eddies shift polewards where the workload is still nearly as great as before.

6. Appendix: Description of EBM3

The full energy balance model EBM3 consists of the diffusive energy balance equation, combined with a theory for the diffusivity. The full equation in steady state is

$$S - I + \frac{\tilde{D}}{a^2 cos(\phi)} \frac{d}{d\phi} \left(cos(\phi) \frac{dm}{d\phi} \right) = 0 \tag{13}$$

where m is the surface moist static energy, S is the solar heating, I is the longwave cooling, $\tilde{D}$ is the diffusivity, a is the Earth's radius, and ϕ is the latitude. The solar heating S is specified to be the same as in the GCM. The longwave cooling I is calculated from the temperature at the emission level, i.e.,

$$I = \sigma T(z_E)^4 \tag{14}$$

with the emission level z_E given by the approximation in equation 9. The temperature at the emission level is calculated from the surface moist static energy assuming a surface relative humidity of 80%, and moist adiabatic temperature structure throughout the troposphere. The moist adiabatic approximation is used in all aspects of the energy balance model.

The diffusivity $\tilde{D}$ is calculated as proportional to a length scale and an eddy velocity scale with a constant of proportionality (discussed later):

$$\tilde{D} = k p_s L |v'| / g. \tag{15}$$

The length scale L is the Rhines scale at latitude of maximum eddy kinetic energy,

$$L = L_0 (|v'| / \beta(\phi_0))^{1/2} \tag{16}$$

where ϕ_0 is the latitude of maximum eddy kinetic energy and β is the meridional gradient of the Coriolis parameter. The velocity scale is proportional to the temperature gradient at 4 km divided by the Coriolis parameter, all at the latitude of maximum eddy kinetic energy:

$$|v'| = \frac{v_0}{f(\phi_0)} \frac{\partial T_{4000}}{\partial y}. \tag{17}$$

Combining expressions 15, 16, and 17, we obtain the full expression for the diffusivity

$$\tilde{D} = D_0(f(\phi_0))^{-3/2}(\beta(\phi_0))^{-1/2}\left(\frac{\partial T_{4000}}{\partial y}\right)^{3/2} \tag{18}$$

where all relevant constants have been gathered into the constant D_0. The temperatures at 4 km are calculated from the surface moist static energy by assuming moist adiabatic ascent. Finally, we obtain the latitude of maximum eddy kinetic energy by locating the maximum temperature gradient at 4 km.

We run the model with 1000 grid points equally spaced in latitude, and integrate the equations in time until a steady state is reached. The diffusivity coefficient D_0 is calculated by tuning the flux in the control case to match the GCM value.

References

Barry, L., G. C. Craig, and J. Thuburn: 2002, Poleward heat transport by the atmospheric heat engine. *Nature*, **415**, 774–777.

Branscome, L. E.: 1983, A parameterization of transient eddy heat flux on a beta-plane. *J. Atmos. Sci.*, **40**, 2508–2521.

Budyko, M. I.: 1969, The effect of solar radiation variations on the climate of the earth. *Tellus*, **21**, 611–619.

Cabellero, R. and P. L. Langen: 2005, The dynamic range of poleward energy transport in an atmospheric general circulation model. *Geophys. Res. Lett.*, **32**, L2705, doi:10.1029/2004GL021581.

Charney, J. and A. Eliassen: 1964, On the growth of the hurricane depression. *J. Atmos. Sci.*, **21**, 68–75.

Frierson, D. M. W.: 2006, The dynamics of idealized convection schemes and their effect on the zonally averaged tropical circulation. *Submitted to J. Atmos. Sci.*.

Frierson, D. M. W., I. M. Held, and P. Zurita-Gotor: 2006, A gray-radiation aquaplanet moist GCM. Part I: Static stability and eddy scale. *In press, J. Atmos. Sci.*.

Green, J. S.: 1970, Transfer properties of the large scale eddies and the general circulation of the atmosphere. *Quart. J. Roy. Meteor. Soc.*, **96**, 157–185.

Haine, T. W. N. and J. Marshall: 1998, Gravitational, symmetric, and baroclinic instability of the ocean mixed layer. *J. Phys. Oceanogr.*, **28**, 634–658.

Held, I. M. and B. J. Hoskins: 1985, Large-scale eddies and the general circulation of the troposphere. *Advances in Geophysics*, **28**, 3–31.

Held, I. M. and V. D. Larichev: 1996, A scaling theory for horizontally homogeneous, baroclinically unstable flow on a beta plane. *J. Atmos. Sci.*, **53**, 946–952.

Hoskins, B. J. and P. J. Valdes: 1990, On the existence of storm tracks. *J. Atmos. Sci.*, **47**, 1854–1864.

Lapeyre, G. and I. M. Held: 2003, Diffusivity, kinetic energy dissipation, and closure theories for the poleward eddy heat flux. *J. Atmos. Sci.*, **60**, 2907–2916.

Manabe, S., K. Bryan, and M. J. Spelman: 1975, A global ocean-atmosphere climate model. Part I. The atmospheric circulation. *J. Phys. Oceanogr.*, **5**, 3–29.

Manabe, S., J. Smagorinsky, and R. F. Strickler: 1965, Simulated climatology of a general circulation model with a hydrologic cycle. *Mon. Wea. Rev.*, **93**, 769–798.

Manabe, S. and T. B. Terpstra: 1974, The effects of mountains on the general circulation of the atmosphere as identified by numerical experiments. *J. Atmos. Sci.*, **31**, 3–42.

Neelin, J. D. and I. M. Held: 1987, Modeling tropical convergence based on the moist static energy budget. *Mon. Wea. Rev.*, **115**, 3–12.

Pavan, V. and I. M. Held: 1996, The diffusive approximation for eddy fluxes in baroclinically unstable jets. *J. Atmos. Sci.*, **53**, 1262–1272.

Pierrehumbert, R. T.: 2002, The hydrologic cycle in deep-time climate problems. *Nature*, **419**, 191–198.

Schneider, T.: 2004, The tropopause and the thermal stratification in the extratropics of a dry atmosphere. *J. Atmos. Sci*, **61**, 1317–1340.

Sellers, W. D.: 1969, A climate model based on the energy balance of the earth-atmosphere system. *J. Appl. Meteor.*, **8**, 392–400.

Stone, P. H.: 1972, A simplified radiative-dynamical model for the static stability of rotating atmospheres. *J. Atmos. Sci*, **29**, 405–418.

— 1978, Constraints on dynamical transports of energy on a spherical planet. *Dyn. Atmos. Oceans*, **2**, 123–139.

Stone, P. H. and M.-S. Yao: 1990, Development of a 2-dimensional zonally averaged statistical-dynamic model. 3. The parameterization of eddy fluxes of heat and moisture. *J. Climate*, **3**, 726–740.

Trenberth, K. E. and J. M. Caron: 2001, Estimates of meridional atmosphere and ocean heat transports. *J. Climate*, **14**, 3433–3443.

Trenberth, K. E. and D. P. Stepaniak: 2003a, Covariability of components of poleward atmospheric energy transports on seasonal and interannual timescales. *J. Climate*, **16**, 3691–3705.

— 2003b, Seamless poleward atmospheric energy transports and implications for the Hadley Circulation. *J. Climate*, **16**, 3706–3722.

Yin, J. H.: 2005, A consistent poleward shift of the storm tracks in simulations of 21st century climate . *Geophys. Res. Lett.*, **32**, L18701, doi:10.1029/2005GL023684.

List of Tables

List of Figures

Table 1: Partition of vertically integrated moist static energy fluxes into sensible and latent components at the latitude of maximum flux (ϕ_{max}) for the T170 simulations. Units are $PW = 10^{15}\ W$ for all simulations.

Simulation	ϕ_{max}	MSE flux	DSE flux	Moisture flux	Compensation
$\xi = 0$	35.4	5.61	5.61	0	
$\xi = 1$	36.1	5.64	2.95	2.69	98.9%
$\xi = 10$	36.8	6.03	0.09	5.94	92.9%

Table 2: Partition of vertically integrated moist static energy fluxes into sensible and latent components at the latitude of maximum flux (ϕ_{max}) for the T85 simulations. Units are PW for all simulations.

Simulation	ϕ_{max}	MSE flux	DSE flux	Moisture flux	Compensation
$\xi = 0$	35.7	5.61	5.61	0	
$\xi = 0.5$	35.7	5.85	3.99	1.86	87.1%
$\xi = 1$	35.7	5.87	2.95	2.92	91.1%
$\xi = 2$	37.1	5.85	1.93	3.93	93.6%
$\xi = 4$	37.1	6.00	1.11	4.89	92.0%
$\xi = 10$	37.1	6.40	0.19	6.21	87.3%

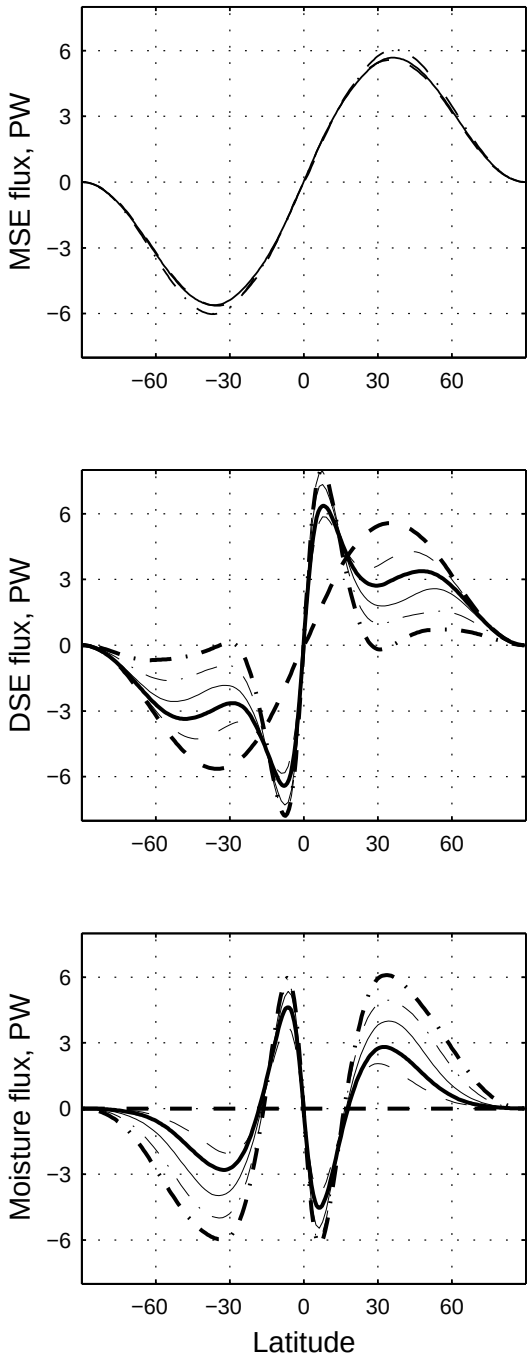

Figure 1: Vertically integrated energy transports for the T170 cases (thicker lines): control case (solid), dry limit (dashed), and 10X case (dash-dot). (a) Moist static energy, (b) Dry static energy, and (c) Moisture. Additionally plotted in (b) and (c) are the T85 cases (thinner lines): .5X case (dashed), 2X case (solid), and 4X case (dash-dot). Units are PW $(10^{15}\ W)$.

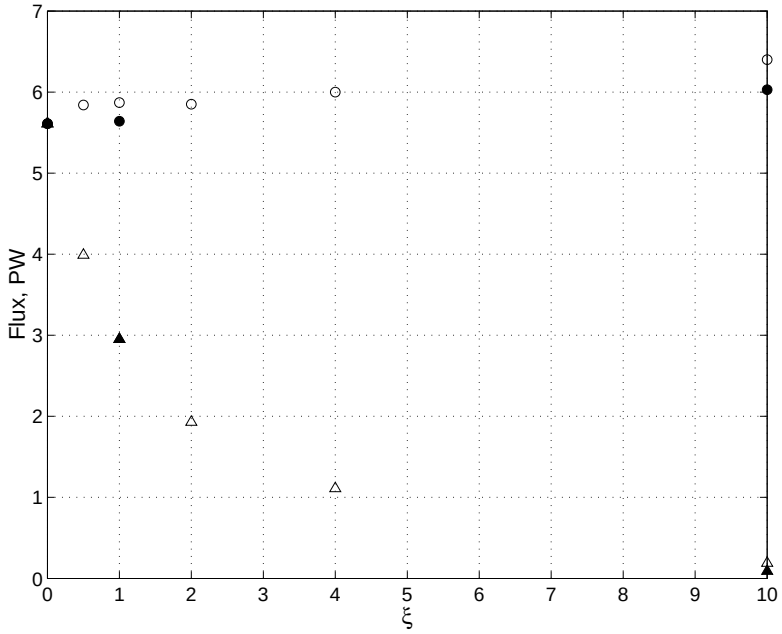

Figure 2: Vertically integrated moist static energy flux (circles) and dry static energy flux (triangles) at the latitude of maximum moist static energy flux as a function of the moisture content parameter ξ. T170 simulations (filled), T85 simulations (open). Units are PW.

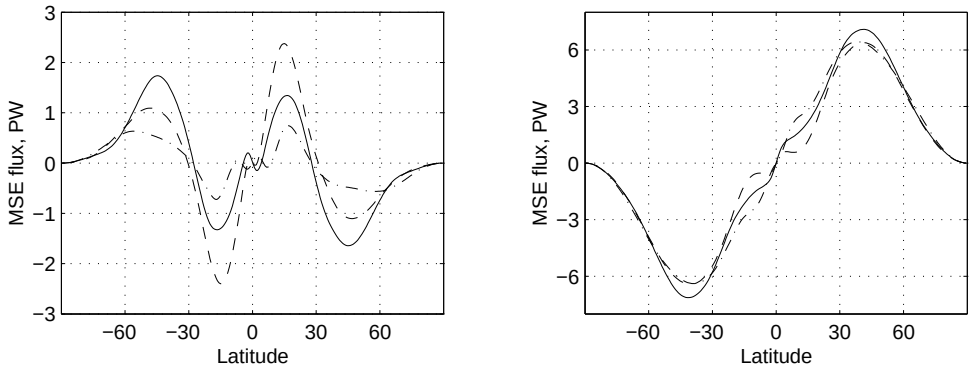

Figure 3: Vertically integrated moist static energy transport (a) by the mean flow and (b) by eddies for the control case (solid), dry limit (dashed), and 10X case (dash-dot), all at T170 resolution. Units are PW for all simulations. Note the different scales for each plot.

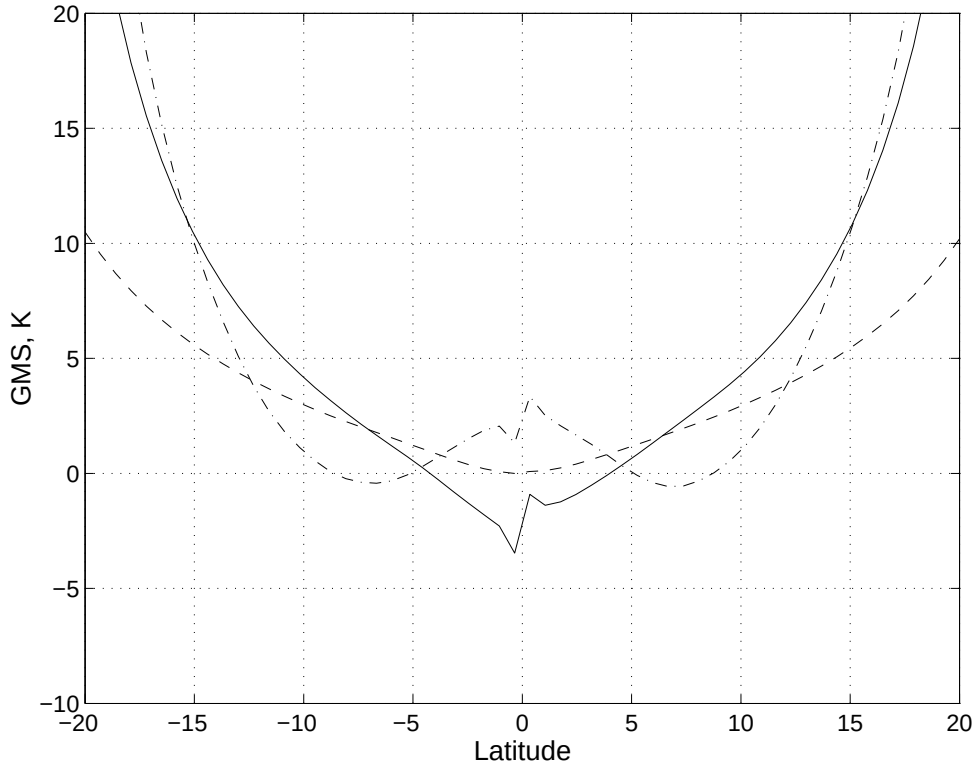

Figure 4: Gross moist stability for the control case (solid), the dry limit (dashed), and the 10X case (dash-dot), all at T170 resolution (units of temperature in K).

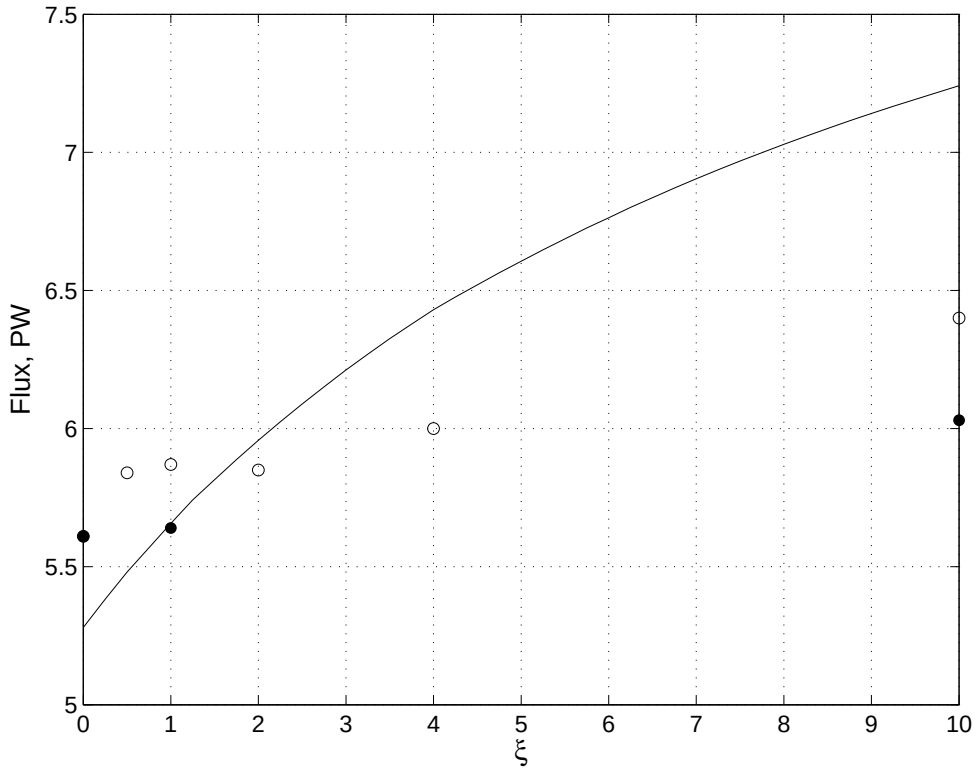

Figure 5: Maximum MSE fluxes as a function of the moisture content parameter ξ for the GCM T170 simulations (filled circles), the GCM T85 simulations (open circles), and EBM2 (solid line).

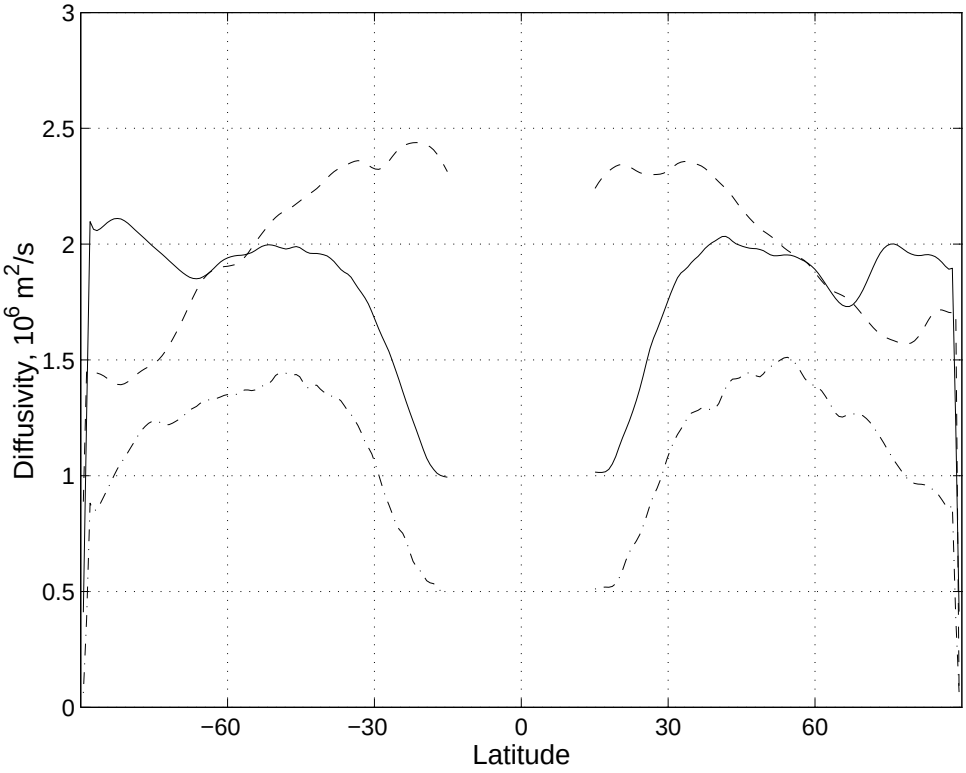

Figure 6: Effective diffusivities from the GCM (solid=control, dashed=dry limit, dash-dot=10X case, units are $10^6\ m^2\ s^{-1}$).

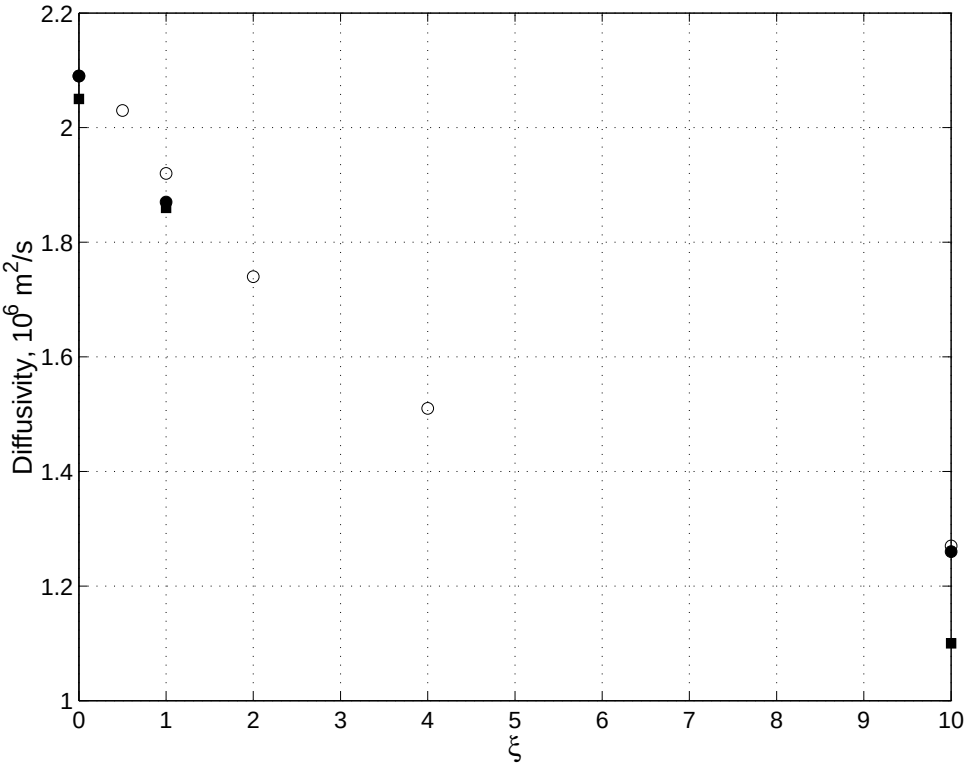

Figure 7: Mean effective diffusivities (averaged poleward of 25 degrees) from the GCM as a function of moisture content ξ, and the diffusivity required in EBM2 to reproduce the GCM maximum MSE flux (filled circles=T170, open circles=T85, squares=required EBM2 diff, units are $10^6\ m^2\ s^{-1}$).

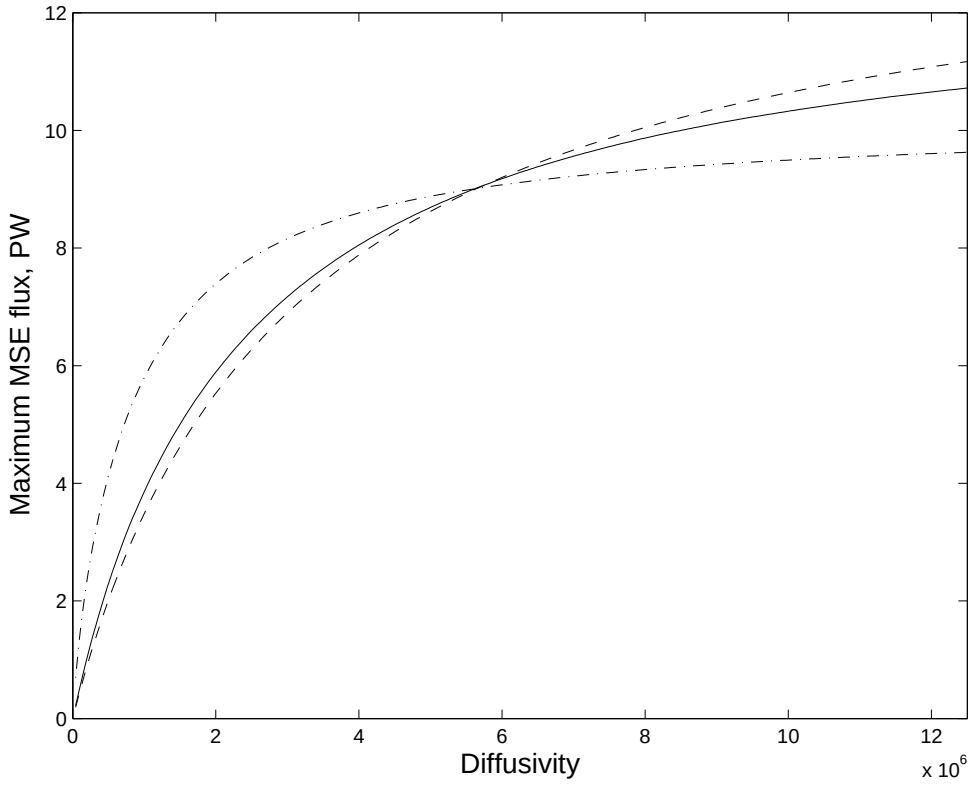

Figure 8: Maximum flux (in PW) varying diffusivity (in $m^2\ s^{-1}$) in EBM2 for the control simulation (solid), dry limit (dashed), and 10X case (dash-dot).

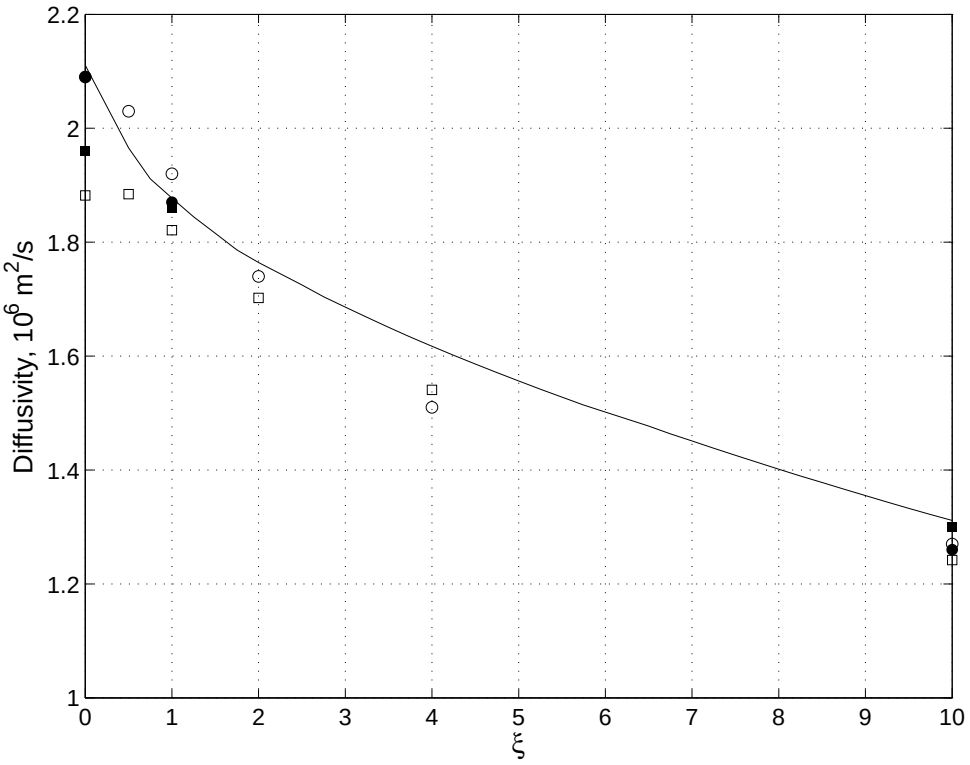

Figure 9: Mean diffusivities from the GCM (filled circles=T170, open circles=T85), the predicted diffusivities from $D = LV$ in the GCM at T170 (filled squares) and T85 (open squares), and the diffusivity from EBM3 (solid). Units are $10^6\ m^2\ s^{-1}$.

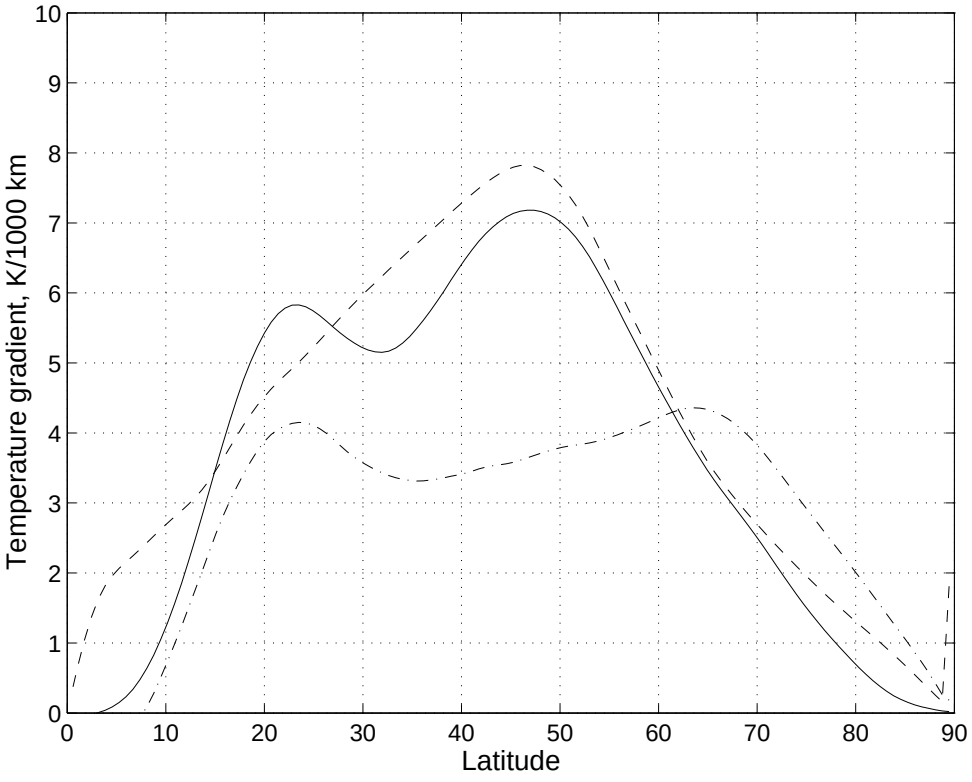

Figure 10: Meridional temperature gradients at 630 hPa, in $K/1000\ km$ (solid=control case, dashed=dry limit, dash-dot=10X case).

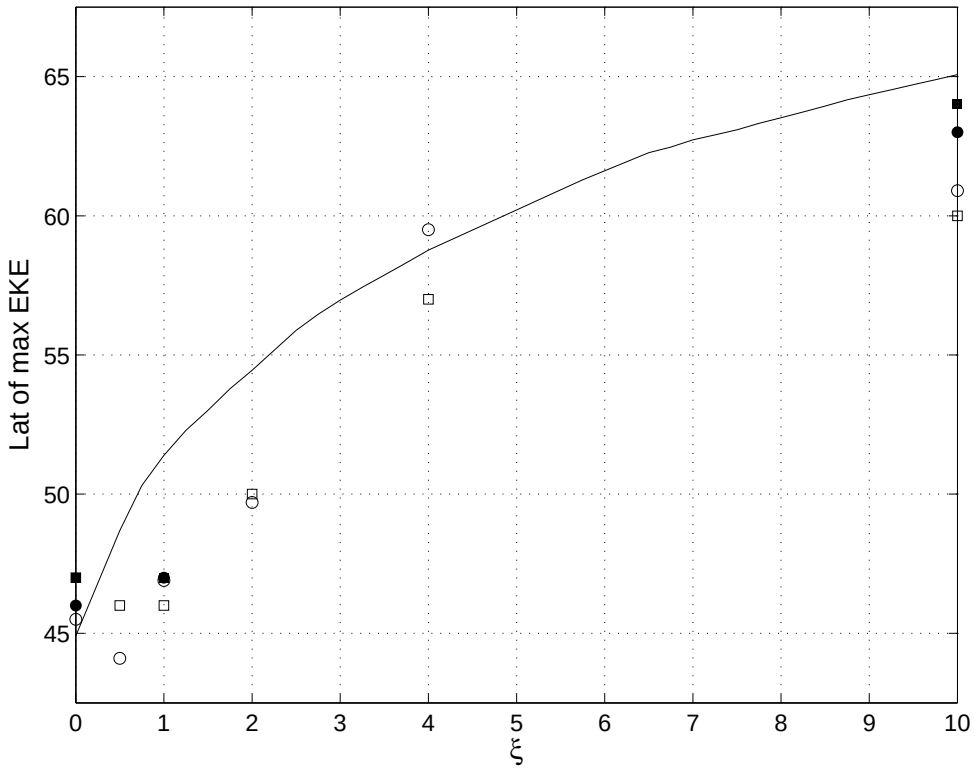

Figure 11: Latitude of maximum eddy kinetic energy from the GCM (filled circles=T170, open circles=T85), the predicted latitudes from the theory at T170 (filled squares) and T85 (open squares), and from EBM3 (solid).

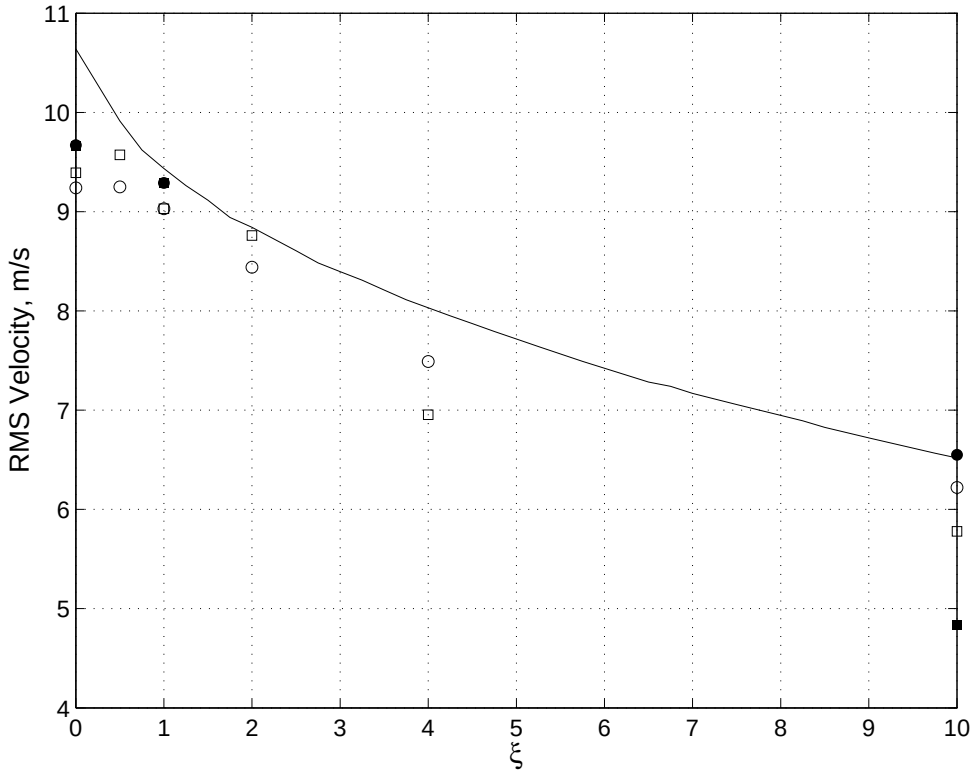

Figure 12: RMS velocity from the GCM (filled circles=T170, open circles=T85), the predicted velocities from the theory at T170 (filled squares) and T85 (open squares), and from EBM3 (solid).

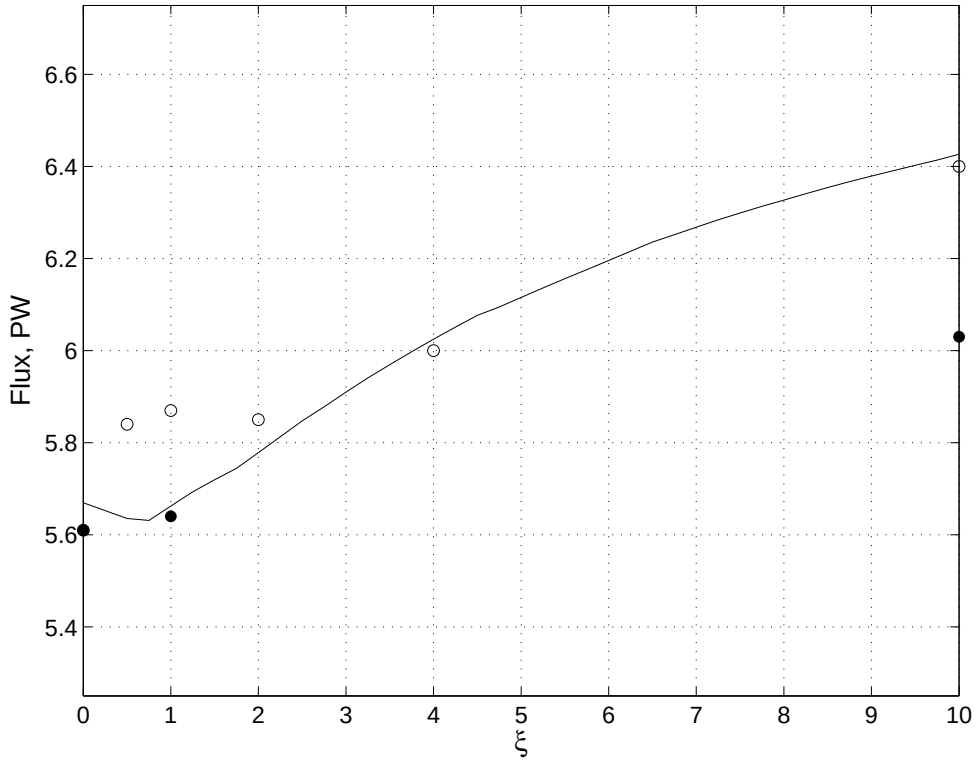

Figure 13: Maximum moist static energy flux from the GCM (filled circles=T170, open circles=T85), and predicted flux from EBM3 (solid).